Mercury emission from industrially contaminated soils in relation to chemical, microbial, and meteorological factors☆

Stefan Osterwalder [a, b, *], Jen-How Huang [a], Waleed H. Shetaya [a, c], Yannick Agnan [d], Aline Frossard [e], Beat Frey [e], Christine Alewell [a], Ruben Kretzschmar [f], Harald Biester [g], Daniel Obrist [h]

[a] Environmental Geosciences, University of Basel, 4056 Basel, Switzerland
[b] Department of Forest Ecology and Management, Swedish University of Agricultural Sciences, 901 83 Umeå, Sweden
[c] Air Pollution Research Department, Environmental Research Division, National Research Centre, Dokki, Giza 12622, Egypt
[d] Sorbonne Université, CNRS, EPHE, UMR Metis, 75252 Paris, France
[e] Federal Research Institute WSL, 8903 Birmensdorf, Switzerland
[f] Institute of Biogeochemistry and Pollutant Dynamics, CHN, ETH Zürich, Zürich, Switzerland
[g] Institut für Geökologie, AG Umweltgeochemie, Technische Universität Braunschweig, 38106 Braunschweig, Germany
[h] Department of Environmental, Earth and Atmospheric Sciences, University of Massachusetts, Lowell, MA 01854, USA

Keywords:
Air-surface exchange
Flux
Soil
Contamination
Bacteria
merA

A B S T R A C T

The Minamata Convention entered into force in 2017 with the aim to phase-out the use of mercury (Hg) in manufacturing processes such as the chlor-alkali or vinyl chloride monomer production. However, past industrial use of Hg had already resulted in extensive soil pollution, which poses a potential environmental threat. We investigated the emission of gaseous elemental mercury (Hg^0) from Hg polluted soils in settlement areas in the canton of Valais, Switzerland, and its impact on local air Hg concentrations. Most soil Hg was found as soil matrix-bound divalent Hg (Hg^{II}). Elemental mercury (Hg^0) was undetectable in soils, yet we observed substantial Hg^0 emission (20−1392 ng m^{-2} h^{-1}) from 27 soil plots contaminated with Hg (0.2−390 mg Hg kg^{-1}). The emissions of Hg^0 were calculated for 1274 parcels covering an area of 8.6 km^2 of which 12% exceeded the Swiss soil remediation threshold of 2 mg Hg kg^{-1}. The annual Hg^0 emission from this area was approximately 6 kg a^{-1}, which is almost 1% of the total atmospheric Hg emissions in Switzerland based on emission inventory estimates. Our results show a higher abundance of Hg resistance genes (*merA*) in soil microbial communities with increasing soil Hg concentrations, indicating that biotic reduction of Hg^{II} is likely an important pathway to form volatile Hg^0 in these soils. The total soil Hg pool in the top 20 cm of the investigated area was 4288 kg; hence, if not remediated, these contaminated soils remain a long-term source of atmospheric Hg, which is prone to long-range atmospheric transport.

1. Introduction

The global threat posed by mercury (Hg) pollution united over 120 nations to sign the legally binding framework of the Minamata Convention on Mercury (UNEP, 2013). This protocol has entered into force in August 2017, and aims to reduce both Hg use and global anthropogenic Hg emissions to the atmosphere. Today, global anthropogenic Hg emissions account for 2500 ± 500 t a^{-1} (Outridge et al., 2018). Artisanal and small-scale gold mining has been identified as the major source of anthropogenic Hg emission to the atmosphere (>800 t a^{-1}), followed by industrial activities such as manufacture of non-ferrous metals or cement production (>500 t a^{-1}), stationary combustion (>500 t a^{-1}), intentional use of Hg (>200 t a^{-1}), and waste disposal and incineration (>100 t a^{-1}) (UNEP, 2019). The phase-out under the Minamata convention of the industrial use of Hg is expected to decrease Hg emissions (EU, 2017); however, the surroundings of some chemical factories subjected to severe Hg pollution in the past carry significant legacies, mainly due to Hg dispersion around production buildings and in

wastewater discharge (Amos et al., 2013). After closure of a base-metal smelter in Canada, soils in the area switched from being a net sink for atmospheric Hg during operation, to a net source with a daily mean emission flux of 108 ng m^{-2} h^{-1} (Eckley et al., 2015). The authors estimated that contaminated soils within 50 km of the smelter (<100 mg Hg kg^{-1}) emitted almost 100 kg Hg a^{-1} to the air. Zhu et al. (2018) reported elevated surface soil Hg concentrations (<4.8 mg kg^{-1}) within a 6.5-km radius from a closed industrial plant in China and concluded that legacy emission of gaseous elemental mercury (Hg^0) is in the same order as from naturally enriched mines. Higher levels of Hg (>10 mg kg^{-1}) have been located in soils in the vicinity (<5 km radius) of a Czech chlor-alkali plant (Suchara and Sucharová, 2008; Grangeon et al., 2012; Guédron et al., 2013; Navratil et al., 2017) that is a long-term source of Hg to the air, water, and eventually biota if not managed properly. Mercury in wastewater discharge from a chlor-alkali plant in Portugal was the source for strong soil Hg contamination in the range of 1 to 91 mg kg^{-1} (Reis et al., 2009).

Legacy Hg pollution, including that contained in soils contaminated by industrial activities, will likely continue to be an environmental threat even after a complete phase-out of industrial use of Hg (UNEP, 2019; Horowitz et al., 2014). Global emissions of Hg from contaminated, naturally-enriched and mining sites are estimated to be 217 t a^{-1} (median) and range from 202 to 258 t a^{-1} (Agnan et al., 2016). Nonetheless, emissions from contaminated sites are not accounted for in actual emission inventories because they have not been reliably quantified. As such, estimation of atmospheric Hg^0 emission from industrially contaminated soils, are associated with large uncertainties (globally between 14 and 34 t a^{-1}, Kocman et al., 2013) mainly due to a lack of direct Hg^0 emission measurements (Kim and Kim, 1999; Wallschläger et al., 2002; Rinklebe et al., 2009; Eckley et al., 2015; Zhu et al., 2018). Emission of Hg^0 from soils with elevated Hg levels are dominantly controlled by total mercury (THg) concentrations in the soil (e.g. Edwards et al., 2001; Frescholtz and Gustin, 2004; Wang et al., 2005). Based on a compilation of 538 direct flux measurements, emission of Hg^0 from Hg-enriched sites (>0.3 mg kg^{-1}) showed a strong linear correlation with soil THg concentrations ($\rho = 0.608$, $p < 0.01$) (Agnan et al., 2016).

The main objectives of this study were to identify the Hg^0 emissions from contaminated oxic soils from settlement areas of Visp and Turtig-Raron in Switzerland (Canton of Valais) and relate these findings to soil Hg speciation measurements presented in Gilli et al. (2018). Previous studies at these sites have shown that most soil Hg resides in relatively stable pools (e.g. Shetaya et al., 2017) strongly bound to soil solids ("matrix-bound Hg^{II}"), most likely associated with organic matter and that Hg^0 was not detectable by thermal desorption analysis (Gilli et al., 2018; Grigg et al., 2018). We hypothesize that instantaneous Hg^{II} reduction in the large soil Hg pool (0.5–28.5 mg kg^{-1}, Gilli et al., 2018) can still drive outgassing of Hg^0 even though soil Hg^0 concentrations are low. In order to measure Hg^0 emissions, we performed dynamic flux chamber experiments in shaded conditions to eliminate the effects of solar radiation, which is known to strongly promote Hg^0 evasion through photochemical reduction (Moore and Carpi, 2005). This allowed to better investigate the potential role of microbial *mer*A genes on Hg^{II} reduction and subsequent Hg^0 emissions in soils. Bacteria and archaea have evolved resistance mechanisms to Hg (Hg resistant *mer* system) that degrade organic Hg and detoxify Hg^{II} by reduction to Hg^0, effectively partitioning Hg^0 to the gaseous phase (Barkay et al., 2003; Lin et al., 2011). In addition, we assessed the relationship between soil THg concentrations and Hg^0 emission potential, the pollution potential of Hg in the contaminated sites in this area, and estimated the atmospheric Hg emissions of the area in relation to other atmospheric emission sources.

2. Materials and methods

2.1. Study area and contamination history

We focused our research on nine Hg contaminated parcels located in settlement areas of the towns Visp (658 m a. s. l.) and Turtig-Raron (638 m a. s. l.), Canton of Valais, Switzerland. The study area is characterized by a dry climate typical for inner-alpine valleys, because they are sheltered against precipitation from both the north and the south. The 30-year (1981–2010) annual mean precipitation in the area is 596 mm with no distinct rainy or dry seasons and the mean annual temperature is 9.4 °C. January and July monthly mean temperatures are 1.3 °C and 19.3 °C, respectively. During convective weather situations, valley breezes from the west develop during the day, whereas mountain breezes from the east dominate during the night.

The the soil Hg contamination within the investigated area spreading over 8.6 km^2 is mainly associated with the drainage canal (the "Grossgrundkanal") that runs through a chemical manufacturing facility in Visp (Fig. 1). Since 1917, Hg has been used as a catalyst during the production of acetaldehyde, vinyl acetate, vinyl chloride, and also in the chlor-alkali electrolysis on the chemical production area in Visp (ForumUmwelt, 2011). Between about 1930 and 1976, Hg contaminated water carrying 50–200 tons of Hg was directed into the canal and contaminated the canal sediments. An additional 50 tons of Hg^0 were emitted to the air. The sediments were regularly dredged and then spread as fertilizer on agricultural soils and gardens or were used as fill material in settlement areas until 1990 (ForumUmwelt, 2011). In 2012, the environmental agency of the canton of Valais (in German Dienststelle für Umwelt, DUW) required soil investigation in order to assess the extension of the polluted area. In total, more than 3500 soil samples (0–20 cm) on 1274 parcels were taken since the beginning of the investigations (DUW, pers. communication). Sampling and analysis of THg concentrations followed the Swiss standard regulations on soil pollution protocol (Swiss VBBo procedures; VBBo, 1998).

2.2. Ambient Hg^0 concentration and soil-air Hg^0 flux measurements

For this study, we have re-visited nine parcels (T-S1, T-S3, T-S8, T-S11, V-S4, V-S5, V-S6, V-S7, V-S8) with soil THg concentrations previously determined ranging from <0.1 to 210 mg kg^{-1} (see Table S1). We distinguished three land cover types of the parcels: lawn (T-S1, T-S11, V-S4, V-S5, V-S6), grassland (T-S3, T-S8, V-S7), and bare soil (V-S8). At each parcel, Hg^0 flux was measured over three plots alternately during a 24-h period between August 16 and 29, 2015 (as such having $n = 27$ concentration and flux measurements). The plots were chosen randomly within an area of 10 m × 10 m or along a line-transect. During one day our new type dynamic flux chamber (DFC) described in Lin et al. (2012) and applied by Osterwalder et al. (2018) was placed eight times on the same plot for 40 min; between the measurements, the DFC was cleaned with ultrapure water (Milli-Q, 18.2 MΩ cm, Millipore Corp.) and dried. The new DFC type was applied because its design enables a uniform airstream inside the chamber and accounts for the effect of atmospheric turbulence and has yielded cumulative flux values similar to the turbulent fluxes (Osterwalder et al., 2018). Thus, a representative flux under ambient atmospheric conditions was inferred from the measured DFC flux multiplied by the ratio of the overall transfer coefficient under ambient atmospheric conditions and the overall mass transfer coefficient in the DFC (Eq. (1)). Using a synchronized dual-port sampling unit (Tekran® Model 1110, Toronto, ON, Canada) the inlet and outlet air from the DFC was sampled and analyzed for Hg^0 by a Tekran® 2537A instrument (see Fig. S1). The inlet ambient Hg^0 concentration was measured just

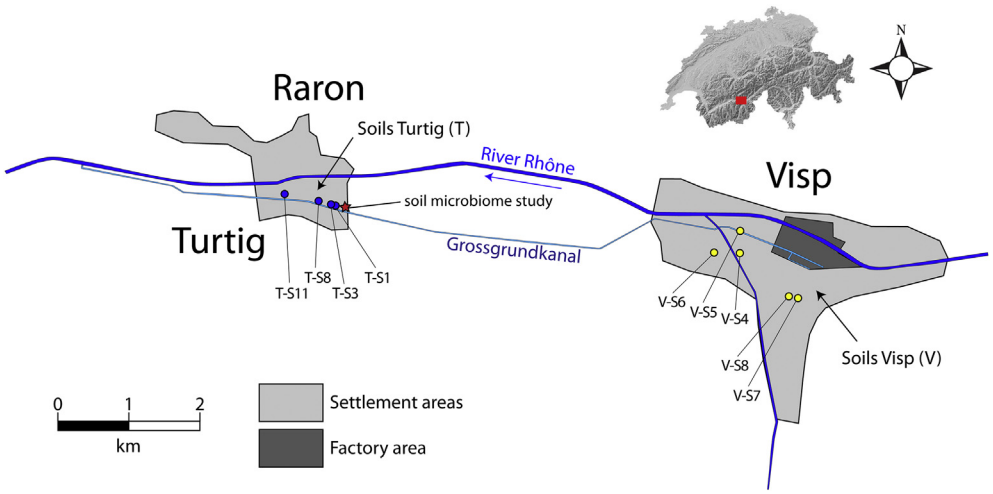

Fig. 1. Schematic map of the area where ambient Hg^0 concentration and Hg^0 flux measurements were performed and subsequently soil samples were taken with respect to the regional Swiss map. Blue circles represent study sites within the settlement area in Turtig-Raron and yellow circles within Visp. The red star indicates the location of soil collection to study abundance of the Hg resistance genes. Direction of surface water flow in both the Grossgrundkanal and the River Rhône is from right to left. Base map is courtesy of the Swiss Federal Office of Topography (Swisstopo).

above the DFC air entrance zone (l × w = 0.1 m × 0.3 m). The air entrance zone was open to above, clearly separated from the lawn canopy and within the turbulent boundary layer (see Fig. S1). The sampling interval of the air Hg analyzer was 10 min (two 5-min samples) at a flow rate of 1.3 L min^{-1}. The flux of Hg^0 (F_{Hg^0}) in ng m^{-2} h^{-1} was calculated according to Equation (1). Positive fluxes indicate Hg^0 emission, negative fluxes Hg^0 deposition, respectively.

$$F_{Hg^0} = \frac{Q(C_i - C_o)}{A} \bullet \frac{k_{atm}}{k} = \frac{Q(C_i - C_o)}{A} \bullet \frac{\left(4.86 + \frac{0.03h^2 u_* D_H/(6kz_0 Dl)}{1+0.016\sqrt[3]{\{(h^2 u_* D_H)/(6z_0 Dl)\}^2}}\right)}{\left(4.86 + \frac{0.03hQD_H/(A_c Dl)}{1+0.016\sqrt[3]{\{(hQD_H)/(A_c Dl)\}^2}}\right)}, \quad (1)$$

where Q is the applied flow rate (0.8 m^3 h^{-1}) through the chamber; C_i and C_o are Hg^0 concentrations of the inlet and outlet air stream (ng m^{-3}); A is the surface area enclosed by the DFC (0.09 m^2); h is the height of the DFC (0.03 m); u^* is the friction velocity (m s^{-1}); D_H and D are the hydraulic radius (0.0545 m) and diffusivity of Hg^0 ($1.194 \cdot 10^{-5}$ m^2 s^{-1}), respectively; k is the Kármán constant (0.41) (Seinfeld and Pandis, 1998); z_0 is surface roughness height (m); l is the distance measured from the starting point of the measurement zone (0.15 m) and A_c is the flow cross-sectional area (0.009 m^2).

The air Hg analyzer was calibrated before and after the field campaign using a temperature-controlled Hg vapor calibration unit (Tekran® Model 2505). Multiple volumes (3–8 μL) of saturated Hg^0 vapor were manually injected into a Hg-free air stream obtained from a zero-air generator (Tekran® Model 1100) using a 10 μL digital gas-tight syringe (Hamilton, Reno, USA). Prior to the field campaign the DFC and all Teflon® PTFE tubing were cleaned with 5% nitric acid and subsequently rinsed with ultrapure water. The DFC blanks were measured in-situ before, during and after the campaign over an acid-cleaned Teflon® PTFE film. The blank average was 2.8 ± 2.4 ng m^{-2} h^{-1} (n = 204) and was subtracted from the flux.

2.3. Soil sampling and analyses

After the Hg^0 flux measurements a topsoil core (0–10 cm) was taken from each plot (i.e., DFC footprint, n = 27) for subsequent soil THg concentration analysis. Additionally, we measured concentrations of the metalloid As, metals such as Co, Cr, Cu, Mo, Ni, Pb, Zn and the elemental concentration of Fe, Al, and Mn in dithionite extracts (see Table S3). Samples were collected using a previously cleaned stainless steel auger and sealed in polyethylene bags for transport. Soils were dried at 40 °C for 48 h and then sieved to <2 mm particle size for analysis. It has been demonstrated by Gilli et al. (2018) that drying of soil samples at 40 °C does not cause evaporation losses of Hg. Soil pH was measured by a glass electrode for 5 min after equilibrating 5 g of the sieved soils (<2 mm) in ultrapure water for 30 min on an end-over-end shaker. A Leco CN 628 analyzer was used to measure soil total organic carbon (TOC) content; 0.25 g of finely ground soils were weighed into tin capsules and combusted at 1000 °C. The TOC concentration was then determined by infrared and thermal conductivity detectors in oxygen-rich and helium environments, respectively.

The dithionite-citrate-bicarbonate extraction method of Kostka and Luther (1994) was used to estimate the concentrations of poorly crystalline (reactive) Fe, Al, and Mn (g kg^{-1}) (Shetaya et al., 2017). Trace metals and metalloid in soil samples were extracted following the VBBo-procedure (VBBo, 1998). In triplicates, 10 g of 2 mm sieved soils were extracted with 100 mL 2 M analytical grade HNO_3 in a boiling water bath for 120 min. Concentrations of metals in the dithionite and acid extracts (diluted in 5% v/v HNO_3) were assayed by an Agilent ICP-OES 5100 and results were processed by the ICP Expert software package. Total Hg in the soil was measured using a Perkin Elmer SMS100 atomic absorption spectrometer according to the EPA standard method 7473. Soil samples were thermally decomposed at 750 °C followed by amalgamation on a gold-trap and then analysis of Hg cold vapors. Certified reference lake sediment material (IAEA SL-1) was used for calibration. Replicate samples and reference material were analyzed regularly (10% of the sampling sequence) and the precision was under 10% relative standard deviation (SD).

2.4. Soil microbial mercury resistance genes (merA)

Samples to investigate the abundance of the Hg resistance genes (merA) were taken from 64 plots in the contaminated site in Turtig-Raron (Fig. 1). After collection from the field, the soil samples were dried at 60 °C and sieved at 2 mm. Total Hg concentrations in soils

were subsequently analyzed using a direct mercury analyzer (AMA 254 Mercury Analyzer, LECO Corporation, St. Joseph, MI, USA; detection limit of 0.001 mg Hg kg^{-1} dw). Total genomic DNA was extracted from 0.5 g sieved soil (2 mm) using the PowerSoil DNA Isolation Kit (MO-BIO Laboratories, Carlsbad, CA, USA). Relative abundances of the mercuric reductase (*merA*)-rRNA copies were determined by quantitative real-time PCR (qPCR) on an ABI7500 Fast Real-Time PCR system (Applied Biosystems, Foster City, CA, USA). PCR amplifications of the merA gene were performed with the MerAF and MerAR primers (Larose et al., 2013). The initial DNA denaturation was at 95 °C for 15 min. Each of the following 40 amplification cycles involved a denaturation step at 95 °C for 30 s, primer annealing at 60 °C for 45 s and an extension phase for 45 s at 72 °C. A final cycle included a denaturation step at 95 °C for 15 s, primer annealing at 60 °C for 1 min followed by denaturation at 95 °C for 15 s qPCR analyses were performed using 2.5 ng DNA in a total volume of 25 μL containing 0.5 μm of each primer, 0.2 mg mL^{-1} BSA and 12.5 μL of QuantiTect SYBR Green PCR master mix (Qiagen, Hirlen, Germany). Three standard curves per target region (correlations ≥ 0.997) were obtained using tenfold serial dilution (10^{-1} to 10^{-9} copies) of plasmids generated from cloned targets (Frey et al., 2011). Data were converted to represent average copy number of targets merA gene per g dry soil.

2.5. Environmental parameters

During the Hg^0 flux measurements, air temperature outside the DFC, relative humidity, wind speed and direction, and precipitation were measured with a weather transmitter (Vaisala WXT520, Vantaa, Finland) mounted onto a mobile tower 2 m above the surface. One meter above the surface, in the shade, solar radiation (Rg), and photosynthetically active radiation (PAR) were measured using a CM11 (Kipp&Zonen, Delft, Netherlands) and a QS5 Quantum Sensor (Delta-T Devices, Cambridge, UK), respectively. In addition to all the other parameters, soil temperature was measured at 2 cm depth with a Campbell Scientific 107 temperature probe and logged every 10 min using a CR1000 (Campbell Scientific, Logan, USA). Soil moisture was determined manually using a ML3 Theta Probe (Delta-T Devices, Cambridge, UK). Air temperature inside the DFC was logged with two DS1923 iButtons (Maxim Integrated, San Jose, USA).

2.6. The global Hg^0 flux database

We compare our Hg^0 flux measurements (n = 27) with global data from Hg-enriched sites (n = 411) presented in Agnan et al. (2016) (called "a global flux database" in the following). According to Agnan et al. (2016) Hg-enriched sites delineate areas where either soil THg concentrations were >0.3 mg kg^{-1} and/or ambient Hg^0 concentrations were >3 ng m^{-3}. Based on this information, Hg-enriched sites were subdivided into four categories: atmospherically influenced (substrate Hg concentration ≤0.3 mg kg^{-1}, but ambient Hg^0 concentration >3 ng m^{-3}), contaminated (i.e., when anthropogenic pollution was indicated), naturally enriched (such as from the geologic Hg mineral belt and geothermal areas), and mining sites (mainly precious-metal mining such as gold, silver, copper). Background sites in the Hg flux database are characterized with soil THg concentrations ≤0.3 mg kg^{-1} and ambient Hg^0 concentrations ≤3 ng m^{-3}. We would like to point out that the Hg^0 flux vs soil THg concentrations relationship for Hg-enriched sites described by Eq. 2 and displayed in Fig. 5 in Agnan et al. (2016) is based on 411 instead of 381 measurements.

3. Results

3.1. Soil properties and total Hg analysis

Soil samples (n = 27) were collected at nine different parcels T-S1, T-S3, T-S8, T-S11, V-S4, V-S5, V-S6, V-S7, V-S8), on three plots each, in Visp and Turtig-Raron (Fig. 1). The soils were weakly acidic to moderately alkaline with pH values ranging, in average, from 6.2 to 8.2 (see Table S3). The TOC content in these soils ranged between 2.6 and 4.5% in average. The concentration of soil THg in all sampling sites spanned from 0.2 to 390 mg kg^{-1} with an interquartile range of 0.4–310 mg kg^{-1} (see Table S2). Soil THg was noticeably elevated (230–390 mg kg^{-1}) in location V-S8 followed by locations T-S3 and T-S8, respectively, indicating high levels of Hg contamination. Depth and spatial heterogeneity in soil THg concentrations are primarily due to uneven distribution of contaminated material or sediments (see Table S2). The Swiss environmental regulation (Ordinance on the Pollution of Soil - VBBo (*ger.*) and Ordinance on contaminated sites - AltlV *(ger.)*) defines three threshold values for soil pollutants. First, the so-called reference value, below which the soil is considered as unpolluted and above which the origin of the contamination has to be identified. Second, the investigation value, above which cantonal authorities are obliged to monitor contaminant development. Third, the remediation value, which enforces either remediation or use restrictions. The reference value for Hg is 0.5 mg kg^{-1}. Since March 2015, the investigation value has been lowered from 2 to 0.5 mg kg^{-1} and the remediation value for settlement areas from 5 to 2 mg kg^{-1} (AltlV, Art. 12 Abs. 1; VBBo, 1998, version 01.05.2017). In all the studied sites, the concentrations of other metals and metalloid did not exceed their respective remediation values (VBBo, 1998). The reference value for Ni (50 mg kg^{-1}) was exceeded at V-S6 and T-S3 and for Pb (50 mg kg^{-1}) at V-S8. The investigation value for Cu (150 mg kg^{-1}) was exceeded up to 2.6 times at V-S8. Moreover, concentrations of Cu, Pb, Zn, and As were significantly correlated to soil THg (r = 0.98, 0.83, 0.65, and 0.35, respectively) indicating a common contamination source (see results from soil properties analysis in Table S3).

3.2. Hg^0 flux from soil and ambient Hg^0 concentrations

During the shaded Hg^0 flux measurement over the 27 plots, air and soil temperatures averaged at 18.9 °C and ranged from 8.7 to 33 °C and 14.9 to 23.6 °C, respectively. The average daytime (≥5 W m^{-2}) solar radiation above the shaded chamber was 51 W m^{-2}. This was always less than 18% of the full daytime solar radiation input measured at the SwissMetNet surface weather station in Visp (VIS S1, 639 m a. s. l.). During the campaign, mostly cloudless conditions prevailed, and there were a few incidents of precipitation (<2 mm). The parcel averaged Hg^0 fluxes ranged between 55 and 1277 ng m^{-2} h^{-1} (see Table S1) and were clearly elevated compared to fluxes (1.2 ± 2.2 ng m^{-2} h^{-1}; average ± SD) measured over background sites with low THg concentrations (Agnan et al., 2016). The largest Hg^0 flux measurement (2114 ng m^{-2} h^{-1}) was observed at site V-S8 over plot 1 (230 mg kg^{-1}) and was more than three orders of magnitude higher compared to background sites. The lowest average Hg^0 flux of 20 ± 13 ng m^{-2} h^{-1} (n = 35) was recorded over plot 3 (0.7 mg THg kg^{-1}) at location V-S7 (Fig. 2a). Overall, 77% of the variability in the observed Hg^0 fluxes is explained by soil THg concentrations according to the linear regression:

$$log_{Flux} = 0.48\, log_{THg} + 1.972 \left(r^2 = 0.77,\ p < 0.001,\ n = 27\right) \quad (2)$$

where log_{Flux} represents the logarithmic Hg^0 flux [ng m^{-2} h^{-1}] and

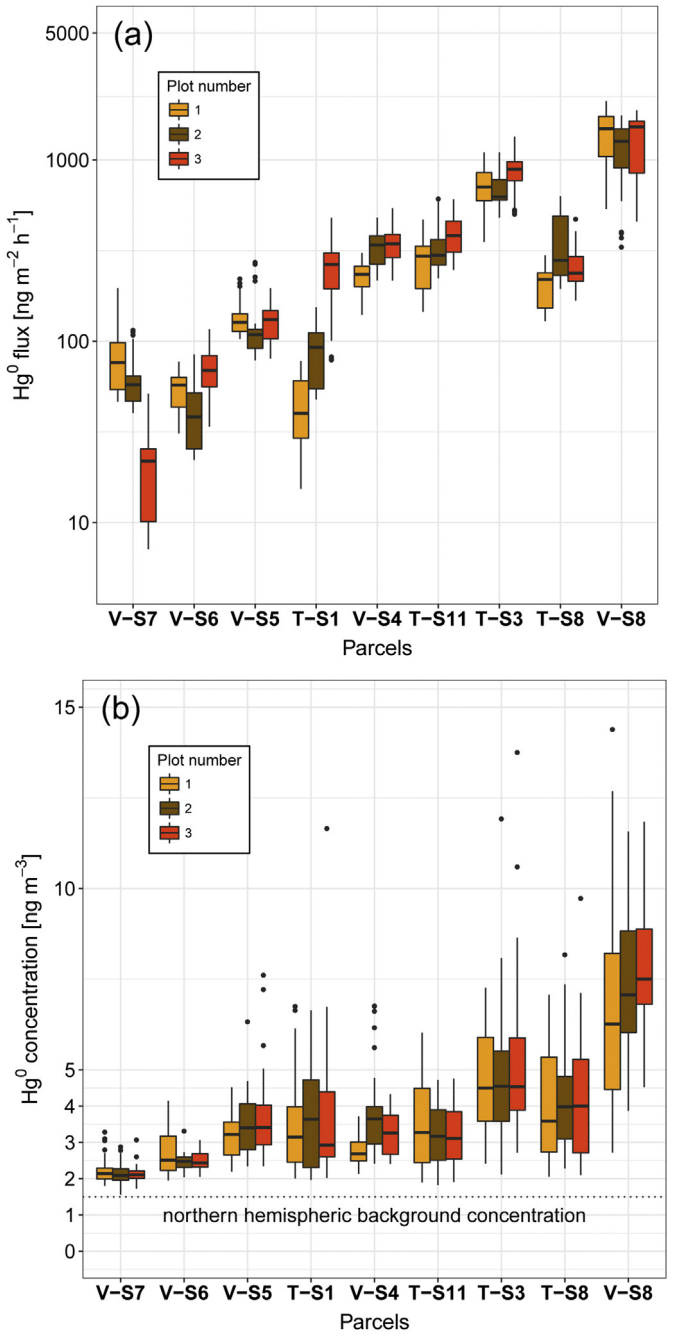

Fig. 2. Box and whisker plots of Hg^0 fluxes (a) and ambient Hg^0 concentrations (b) measured over the plots 1, 2 and 3 (orange, brown, red) at the nine parcels. Boxes contain the middle 50% of the data. The edges of the boxes show the 25th and the 75th percentiles, respectively. The whiskers indicate 1.5 times the interquartile range. Outliers are given as black dots. The largest ambient Hg^0 concentration level of 20.3 ng m^{-3} (T-S3) is not displayed.

log_{THg} the logarithmic soil THg concentrations [mg kg^{-1}].

However, there are parcels where larger Hg^0 fluxes were identified on plots with lower THg concentrations. At V-S7 for example, in about 10 m distance from plot 3, a four times larger flux of 86 ± 42 ng m^{-2} h^{-1} (n = 32) was determined over plot 1 with soil THg concentrations of 0.2 mg THg kg^{-1}. At V-S8, the average Hg^0 flux over plot 1 (1392 ± 485 ng m^{-2} h^{-1}, n = 32) and over plot 3 (1284 ± 486, n = 32) were in a similar range, despite the 41% lower THg concentration found for plot 1. This indicates that even though soil THg is the dominant regulating factor, other parameters might also influence Hg^0 emission. The small-scale heterogeneity of soil contamination was reflected at site T-S8. There, the soil THg concentration measurement, which followed the VBBo extraction protocol, was 79 mg kg^{-1} but ranged from 12 to 26 mg kg^{-1} on plots 1–3 using the total digestion method (see Table S2).

The daily average ambient Hg^0 concentrations measured at each parcel ranged from 2.2 to 7.3 ng m^{-3} (Fig. 2b). Hence, the concentrations were elevated by up to a factor of 5.6 compared to a median concentration of 1.3 ng m^{-3} in the atmospheric boundary layer determined at the remote high altitude monitoring station Jungfraujoch, Switzerland (Denzler et al., 2017) and was larger than the northern hemispheric background concentration of ~1.5 ng m^{-3} (Sprovieri et al., 2016). The minimum and maximum recorded values were 1.6 and 20.3 ng m^{-3}, respectively. The positive relationships between the ambient Hg^0 concentration and soil THg concentration (Eq. (3)) and between the ambient Hg^0 concentration and the Hg^0 flux (Eq. (4)) were statistically significant:

$$log_{Hg^0} = 0.158\, log_{THg} + 0.448 \left(r^2 = 0.87,\ p < 0.001,\ n = 27\right) \quad (3)$$

$$log_{Hg^0} = 0.265\, log_{Flux} - 0.053 \left(r^2 = 0.73,\ p < 0.001,\ n = 27\right) \quad (4)$$

Strong positive correlations between ambient Hg^0 and soil THg concentrations and Hg^0 flux indicate that Hg^0 emission directly contributed to elevated ambient Hg^0 concentrations above the contaminated soils in the settlement area in Visp and Turtig-Raron.

3.3. Drivers of Hg^0 emission

Soil THg concentration exerted the dominant control on Hg^0 emission, with a strong linear correlation between the two (r = 0.9, p < 0.001, n = 27). Other parameters such as solar radiation, soil temperature and soil moisture have been reported to modulate Hg^0 evasion over Hg-enriched sites as well (Poissant et al., 1999; Engle et al., 2001; Gustin et al., 2002; Moore and Carpi, 2005; Lin et al., 2010; Zhu et al., 2018). Average daytime ($Rg \geq 5$ W m^{-2}) Hg^0 emissions were 31% higher compared to nighttime fluxes ($Rg < 5$ W m^{-2}), but only 2% (3%) of the overall variability of Hg^0 fluxes were explained by solar radiation (soil temperature) and diel patterns of Hg^0 emissions were small (see Fig. S3). However, we found a combined positive effect of solar radiation - in spite of shading - and soil temperature on Hg^0 evasion that was evidenced by the weak positive correlation between the residuals derived from the linear regression equation soil THg concentration vs. Hg^0 flux and soil temperature as well as daytime solar radiation: $\rho = 0.3$ ($p < 0.05$, n = 852) and $\rho = 0.26$ ($p < 0.05$, n = 468), respectively. Soil moisture showed a weak positive linear correlation with the residuals derived from soil THg concentrations vs. Hg^0 flux regression ($\rho = 0.12$, $p < 0.01$, n = 0.847) (see Fig. S5). Furthermore we quantified the abundance of *merA* gene copy numbers in soil samples taken along a Hg pollution gradient (Fig. 1, red star) from low to high concentrations (0.1–40.5 mg kg^{-1}). During long-term exposure (>60 years), the abundance of *merA* gene copies increased linearly with soil THg concentrations ($\rho = 0.74$, $p < 0.001$, Fig. S2).

3.4. Soil Hg pool concentration

The average topsoil THg concentration (0–20 cm) from all parcels previously analyzed following the VBBo extraction protocol (n = 1274) was 1.8 mg kg^{-1} (10th and 90th percentile of 0.01 and 2.5 mg kg^{-1}, respectively). There were 148 parcels with soil THg concentrations >2 mg kg^{-1}, the threshold above which soil remediation is required. 72.5% of the parcels were categorized as

uncontaminated (<0.5 mg kg^{-1}, please note that we followed the Swiss standard regulations on soil pollution [VBBo, 1998] in defining contamination levels), 15.5% as slightly contaminated (0.5–2 mg kg^{-1}), 5.5% as moderately contaminated (<2–5 mg kg^{-1}) and 6.5% were heavily contaminated (>5 mg kg^{-1}). The Hg pollution potential within the top 20 cm of all the investigated parcels amounted to 4288 kg. This was calculated using a dry soil bulk density of 1400 kg m^{-3} (pers. communication DUW, Canton of Valais).

4. Discussion

4.1. Global Hg^0 flux and ambient Hg^0 concentrations over Hg-enriched sites

Total Hg concentrations in topsoil was the dominant control on Hg^0 emission ($r^2 = 0.77$, $p < 0.001$). This finding is in agreement with data presented in Agnan et al. (2016) from Hg-enriched sites globally ($r^2 = 0.26$, $p < 0.001$, $n = 411$, Fig. 3). The slope between total soil THg concentration and Hg^0 emission (0.48) observed in our study is similar to the slope of 0.427 derived from flux measurements from industrially contaminated, mining, naturally enriched, and atmospherically influenced sites worldwide (Agnan et al., 2016). Hence, there is a 95% probability that the slope of the regression between Hg^0 emissions and natural Hg soil enrichment as documented on the global database by Agnan et al. (2016) encompasses (95% confidence interval: 0.36–0.5) the slope of the regression between Hg^0 emissions and anthropogenic Hg contamination in soils of our investigated area. The average Hg^0 emissions in our study (373 ng m^{-2} h^{-1}) were more than ten times larger compared to average fluxes from contaminated sites in the global database (20 ng m^{-2} h^{-1}) and were comparable to average Hg^0 fluxes from mining sites (Fig. 3). Different soil and meteorological characteristics contribute to a wide range of slopes from Hg^0 flux vs. THg concentration correlations. Exemplarily, larger slopes

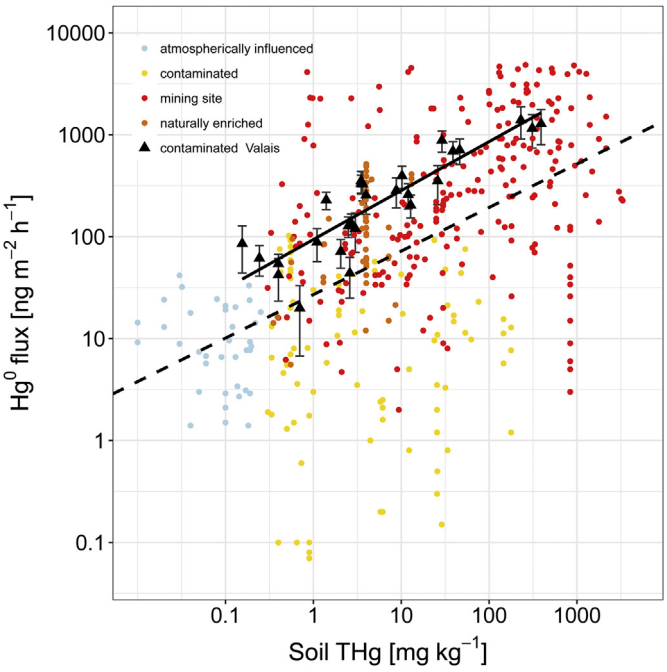

Fig. 3. Relationship between soil THg concentration measurements and average Hg^0 flux in Visp and Turtig-Raron ($n = 27$, black line) and over all Hg-enriched sites in the Hg flux database ($n = 438$, dashed black line). Error bars indicate standard deviation of the Hg^0 flux measured on every plot for 24 h ($n = 8$).

than presented in this study and in Agnan et al. (2016) have been identified in the area of a closed base-metal smelter in Manitoba, Canada and two industrial gold mines in Nevada, USA. In the first case, soil contamination predominantly originated from atmospheric deposition of Hg that lead to strong Hg^0 re-emission: $\log_{Flux} = 0.78 \log_{THg} + 0.39$ ($r^2 = 0.85$) (Eckley et al., 2015). At the Twin Creeks mine and the Cortez-Pipeline mine the regression equations between Hg flux and THg concentration under low solar conditions (<140 W m^{-2}) were $\log_{Flux} = 0.59 \log_{THg} + 2.59$ ($r^2 = 0.66$) and $\log_{Flux} = 0.67 \log_{THg} + 2.49$ ($r^2 = 0.31$) (Eckley et al., 2011). The upscaling exercise revealed that Hg^0 re-emission from the area around the smelter was almost 100 kg a^{-1}, re-emission from the mines was 19 and 109 kg Hg a^{-1}, respectively.

Equation (5) shows an update of the linear regression between Hg^0 fluxes and soil THg concentrations presented in Agnan et al. (2016) by adding our results to the database:

$$log_{Flux} = 0.422 log_{THg} + 1.472 \left(r^2 = 0.26, p < 0.001, n = 438\right) \quad (5)$$

A caveat to this analysis, however, is that we performed our measurement under shaded conditions, while most data from the global database were conducted under natural light conditions, although they likely were highly variable among different studies. Shading was applied to compare fluxes from different parcels independent of the highly variable solar radiation effects. Furthermore, it was helpful to investigate the role of microbial *mer*A genes on Hg^{II} reduction and subsequent Hg^0 emissions in soils; shading also helped to prevent air heating inside the DFC possibly creating an artificial high Hg^0 flux (Eckley et al., 2010) and to avoid measurement bias by shadow casts from buildings and trees surrounding the parcels. The average air temperature within the DFC was only slightly increased compared to ambient air (1 ± 2.2 °C). However, shading the DFC likely also lead to an underestimation of the fluxes during full solar radiation inputs since shading of the DFC suppresses the photochemical reduction of Hg^{II} to Hg^0 at the surface, a process that was reported to be the major driver for higher Hg^0 evasion during daytime (Gustin et al., 2002; Moore and Carpi, 2005; Zhu et al., 2018) (see Sect 3.3).

In this study, Hg^0 emissions from contaminated soils led to elevated ambient Hg^0 concentrations in the lower boundary layer above contaminated soils (Eq. (4)). A similar relationship (slope = 0.39, intercept = 0.49) between Hg^0 flux and ambient Hg^0 concentrations ($r^2 = 0.22$, $p < 0.001$) was found for 230 measurements over Hg-enriched sites (Agnan et al., 2016). The linear regression between Hg^0 flux and ambient Hg^0 concentration over the combined dataset (Fig. 4, black dashed line) showed the following relationship:

$$log_{Hg^0} = 0.331 log_{Flux} + 0.507 \left(r^2 = 0.22, p < 0.001, n = 257\right) \quad (6)$$

In our study the largest ambient Hg^0 concentrations were found to coincide with stable stratification in the nocturnal boundary layer when wind speeds were low and turbulence and vertical mixing suppressed (see Fig. S4). As a result, Hg^0 nighttime concentrations were elevated by 34% on average compared to daytime concentrations. Buildup of a convective mixed layer after sunrise (ca. 06:45) and rising wind speeds in the afternoon were responsible for efficient mixing of accumulated Hg^0 in the atmospheric surface layer and decreases in ambient Hg^0 concentrations.

4.2. Biotic and abiotic drivers of Hg^0 emissions

Despite the lack of detectable Hg^0 in soils based on speciation measurements by thermo-desorption analysis (Gilli et al., 2018), we still observed significant emissions of Hg^0 from these Hg

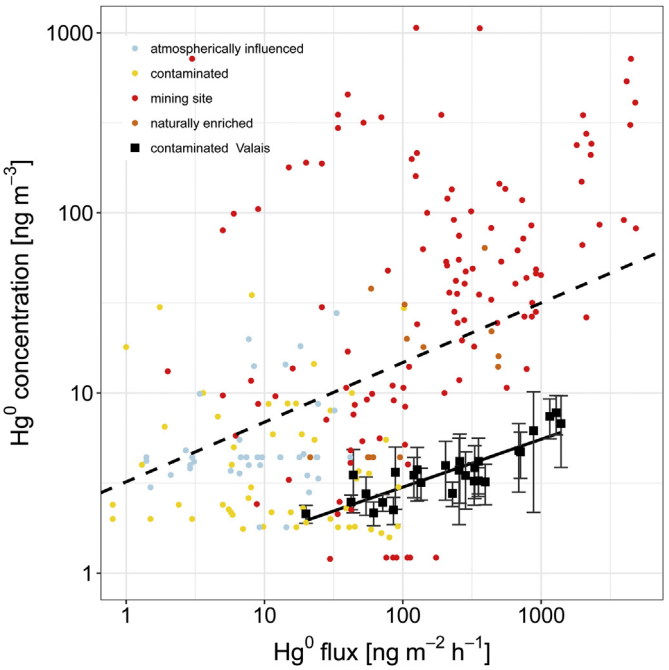

Fig. 4. Relationship between Hg^0 flux and average ambient Hg^0 concentration (n = 27) over all Hg-enriched sites in the Hg flux database (n = 257, dashed black line). Error bars indicate standard deviation of the averaged ambient Hg^0 concentrations measured over every plot during 24 h (n = 8).

contaminated soils. Speciation measurements of soil THg in the investigated contaminated topsoil appears to be consistent with a dominance of Hg-species bound to functional groups of the organic matter (matrix-bound Hg^{II}) (Gilli et al., 2018). However, it is possible that low Hg^0 concentrations existed in soils below the detection limit of the thermo-desorption analysis (0.1 mg kg^{-1}). Observations of substantial Hg^0 emission both during nighttime and under shaded conditions in the absence of detectable Hg^0 in soils suggests a combined role of biological and abiotic Hg^{II} (e.g., photochemical or dark) reduction processes driving subsequent Hg^0 emissions. Based on the difference between nighttime and shaded daytime Hg^0 emissions, we estimate that between 22 and 26% of daytime Hg^0 emissions originated from photochemical reduction of Hg^{II}. Hence, the remaining part of Hg^0 emission likely is associated with abiotic dark reduction and biotic reduction processes.

Abiotic dark reduction is an about 100 times slower process than photochemical Hg^{II} reduction, but is likely more important in soils worldwide (Xiao et al., 1995). However, we suggest that in our oxic soils, biotic reduction of Hg^{II} dominates abiotic dark reduction, a process that has been suggested to occur in sediments, deep waters, and organic-rich soil layers at low redox potentials (Moore and Castro, 2012; Jiang et al., 2015; Jiskra et al., 2015). There are two main pathways of Hg^{II} reduction by bacteria. First, Hg-resistant bacteria reduce Hg^{II} in the cell's cytoplasm using the *mer* operon system. The central (*merA*) gene codes for the mercuric reductase enzyme which catalyzes the reduction from Hg^{II} to Hg^0 (Barkay et al., 2003); Second, Hg-sensitive dissimilatory metal-reducing bacteria use Fe and/or Mn as electron acceptors to reduce Hg^{II} to Hg^0 during respiration (Wiatrowski et al., 2006). In accordance with Dash and Das (2012), we found that the abundance of bacteria with Hg-resistance abilities was proportional to the THg concentration in contaminated soils. Thus, bacterial communities adapted to the long-term Hg pollution without decreasing their functional abilities (Frossard et al., 2018). However, as observed in Frossard et al. (2018), the long-term contamination might have led to a shift of both bacterial and fungal community structure and diversity, while the bacterial abundance remained stable. Microbial reduction of Hg^{II} likely increases with increased Hg contamination, which correlates with observed Hg^0 emissions from these soils. Thus, biotic reduction is important and contributes substantially to Hg^0 emission from contaminated soils.

4.3. Pollution potential and mobilization via Hg^0 emission

Mobility of THg in the soil is largely dependent on the speciation and the way the different species interact with the soil matrix (Biester et al., 2002). Previous investigations on soils in the settlement area revealed that Hg is mainly present as Hg^{II} strongly bound to organic matter (Gilli et al., 2018). Methylmercury (MeHg) concentrations were always below 1% ($\leq$7.8 µg kg^{-1}) of the respective THg contents in the soils (Gilli et al., 2018). The majority of the samples showed around 0.1% MeHg. Shetaya et al. (2017) used an isotope dilution protocol on the soil samples presented herein to estimate the pool of labile Hg, accessible for plants and soil organisms. Despite the wide range of THg values in the soil (0.37–310 mg kg^{-1}), mercury lability spanned a range of ~12–25% highlighting the capacity of surface soils to sequester relatively large quantities of Hg. In another study, the majority of Hg from the soil pool was extracted in the last step using aqua-regia, indicating that little Hg occurred in labile pools (Grigg et al., 2018). Total Hg was strongly bound to soil solids and protected from further reactions.

Our study provides evidence that Hg can also be mobilized from contaminated soils in this area via gaseous Hg^0 emission. This has enabled an empirical estimation of Hg^0 emission from industrially contaminated soils in this region because a large range of soil THg concentrations (0.2–390 mg kg^{-1}) is provided, soil properties are similar (see Table S3) and data comparability is high due to the use of shaded condition and similar weather conditions. In order to constrain the overall Hg^0 emissions from this contaminated area, we estimated a lower level flux (Eq. (7)) describing soil Hg^0 emission during the night (Rg < 5 W m^{-2}) and an upper level shaded daytime flux (average Rg = 51 W m^{-2}; Eq. (8)):

$$log_{Flux_{night}} = 0.486\ log_{THg} + 1.892\ \left(r^2 = 0.73,\ p < 0.001\right) \quad (7)$$

$$log_{Flux_{day}} = 0.479\ log_{THg} + 2.016\ \left(r^2 = 0.78,\ p < 0.001\right) \quad (8)$$

The net annual Hg^0 emission estimate for the entire investigated area of 8.6 km^2 was 6 kg a^{-1} following Equation (2). The lower bound of this estimate is defined by the nighttime flux (Eq. (7)) which is 5 kg a^{-1}. The upper bound of 6.7 kg a^{-1} corresponds to the shaded daytime flux according to Equation (8). Although dense grass cover generally shades soils in this area, it is possible that the upper bound estimate will be higher when direct solar radiation is directly transmitted to barren soil surfaces.

The Hg pollution potential found in upper soils in the investigated settlement area (4.3 tons) accounts for 2–9% of the total amount of Hg potentially released by the factory over the last 100 years (50–200 tons). Assuming that contaminated sediments and soils have existed in this area since 1930 and THg concentrations in topsoil were similar to today, about 500 kg of Hg would have been subject to Hg^0 emission over the years. According to Swiss national CLRTP inventories for Hg emissions, Hg emissions decreased significantly from about 6600 kg a^{-1} in 1990 to 660 kg a^{-1} in 2015 (FOEN, 2017) for the whole of Switzerland. This drop in emissions can be explained by retrofitting the steelworks in the years 1999 and optimization and maintenance of waste incineration plants and

crematoria before 2003. Energy industries contribute 44% of the total Hg emissions to the atmosphere in Switzerland. Emissions from industrial processes, including the chemical industry, contribute 39% (FOEN, 2017). These inventories do not include any diffuse nonpoint sources of Hg^0 emission from contaminated soils in the vicinity of industrial facilities, even though emission from these soils is as large as those measured at Hg mining sites (Fig. 3). Emissions of Hg^0 from the investigated area (8.6 km^2, 0.02% of the national territory) account for about 1% of the total Hg emissions in Switzerland. In comparison, the Hg emission strength of the city of Zurich, the largest city in Switzerland (100 km^2, ca. 400000 inhabitants) has been estimated between 24 ± 8 and 41 ± 8 kg a^{-1} using a boundary-layer budget approach (Denzler et al., 2019). Thus, the amount of diffuse Hg^0 emission from the Visp and Turtig-Raron area is up to 25% of the total emissions from Zurich.

5. Conclusions

Overall, Hg^0 emission measurements over contaminated soils in the Visp and Turtig-Raron settlement areas show that contaminated soils represent a long-term emission source of Hg^0 to the atmosphere. The investigated settlement area of 8.6 km^2 contributed an estimated 6 kg Hg a^{-1} as gaseous elemental Hg^0 emissions to the atmosphere. We found that THg content in the soil had the largest control on Hg^0 emissions ($r^2 = 0.77$, $p < 0.001$). Based on a lack of detectable Hg^0 in soils, Hg^0 emissions likely derived from Hg^{II} reduction in soils. Comparison of daytime and nighttime Hg^0 emissions showed that photochemical reduction processes account for 22–26% of Hg^0 emissions. We propose that microbial communities were likely an important driver for Hg^{II} reduction in these contaminated soils. Evidence for this is based on increasing number of bacterial detoxification genes with increasing soil Hg content, which in turn is linearly correlated with increasing Hg^0 emissions. Since the beginning of the industrial Hg contamination at this site in the 1930, as much as 500 kg of Hg could have been subject to atmospheric Hg^0 emissions, assuming similar soil Hg contamination levels as observed today. Remediation actions such as capping topsoil with 2 cm of low-Hg substrate have been demonstrated to reduce Hg^0 emission by 50–100% at two gold mines in Nevada, US (Miller and Gustin, 2013). Ongoing excavation of contaminated topsoil, however, is the most efficient action to prevent further long-term Hg^0 emissions to the atmosphere that contributes to long-range transboundary air pollution and global atmospheric Hg loads. Ambient Hg^0 concentrations over the investigated parcels in this study ranged between 1.6 and 20.3 ng m^{-3} and were up to 14 times elevated compared to northern hemispheric background concentrations (1.5 ng m^{-3}). However, levels are mostly below the range of acceptable outdoor Hg^0 concentrations of 5–10 ng m^{-3} (WHO, 2000). Thus, air Hg levels in the area were far below the exposure guidelines given by the U.S. EPA reference concentration (300 ng m^{-3}; Carpi and Chen, 2001) or the World Health Organization (200 ng m^{-3}; WHO, 2003). Finally, a report published by the University of Zurich (Dressler and Imo, 2016) found no evidence of adverse health effects to local residents from exposure to Hg in soil or Hg^0 in ambient air in the Visp and Turtig-Raron area.

Acknowledgement

This study was financed by the Dienststelle für Umwelt (DUW) of the Canton of Valais, the Federal Department of Economic Affairs, Education and Research (EAER) and the Freiwillige Akademische Gesellschaft (FAG) Basel. We want to acknowledge Dr. David Trudel from Arcadis Schweiz AG, Dr. Stéphane Westermann and Yves Degoumois from DUW for providing access to their soil THg concentration database, administrative and scientific support. Special thanks go to Jacqueline Riedi for assistance with the dynamic flux chamber measurements and Ramon Hochstrasser (WSL) for quantitative PCR data of *merA* genes. We also wish to thank Dr. Staffan Åkerblom and Prof. Kevin Bishop from the Swedish University of Agricultural Sciences in Uppsala for the soil THg concentration analysis, and Dr. Michael Schmutz and Dr. Roland Vogt from the Atmospheric Science group of the University of Basel for the use of their mobile weather station. The Federal Office of Meteorology and Climatology MeteoSwiss is acknowledged for providing data from the Visp meteorological station.

Appendix A. Supplementary data

Supplementary data to this article can be found online at https://doi.org/10.1016/j.envpol.2019.03.093.

References

Agnan, Y., Le Dantec, T., Moore, C.W., Edwards, G.C., Obrist, D., 2016. New constraints on terrestrial surface-atmosphere fluxes of gaseous elemental mercury using a global database. Environ. Sci. Technol. 50, 507–524.

Amos, H.M., Jacob, D.J., Streets, D.G., Sunderland, E.M., 2013. Legacy impacts of all-time anthropogenic emissions on the global mercury cycle. Glob. Biogeochem. Cycles 27, 410–421.

Barkay, T., Miller, S.M., Summers, A.O., 2003. Bacterial mercury resistance from atoms to ecosystems. FEMS Microbiol. Rev. 27, 355–384.

Biester, H., Müller, G., Schöler, H.F., 2002. Binding and mobility of mercury in soils contaminated by emissions from chlor-alkali plants. Sci. Total Environ. 284, 191–203.

Carpi, A., Chen, Y., 2001. Gaseous elemental mercury as an indoor air pollutant. Environ. Sci. Technol. 35, 4170–4173.

Dash, H.R., Das, S., 2012. Bioremediation of mercury and the importance of bacterial mer genes. Int. Biodeterior. Biodegrad. 75, 207–213.

Denzler, B., Bogdal, C., Kern, C., Tobler, A., Huo, J., Hungerbühler, K., 2019. Urban source term estimation for mercury using a boundary-layer budget method. Atmos. Chem. Phys. Discuss. 19, 3821–3831.

Denzler, B., Bogdal, C., Henne, S., Obrist, D., Steinbacher, M., Hungerbühler, K., 2017. Inversion approach to validate mercury emissions based on background air monitoring at the high altitude research station Jungfraujoch (3580 m). Environ. Sci. Technol. 51, 2846–2853.

Dressler, H., Imo, D., 2016. Gutachten über eine mögliche Gesundheitsgefährdung der Bevölkerung available at: https://www.vs.ch/documents/19415/1246066/Gutachten_Gesundheit_20.06.2016.pdf. (Accessed 20 March 2019).

Eckley, C.S., Blanchard, P., McLennan, D., Mintz, R., Sekela, M., 2015. Soil–air mercury flux near a large industrial emission source before and after closure (Flin Flon, Manitoba, Canada). Environ. Sci. Technol. 49, 9750–9757.

Eckley, C.S., Gustin, M., Lin, C.J., Li, X., Miller, M.B., 2010. The influence of dynamic chamber design and operating parameters on calculated surface-to-air mercury fluxes. Atmos. Environ. 44, 194–203.

Eckley, C.S., Gustin, M., Miller, M.B., Marsik, F., 2011. Scaling non-point-source mercury emissions from two active industrial gold mines: influential variables and annual emission estimates. Environ. Sci. Technol. 45, 392–399.

Edwards, G.C., Rasmussen, P.E., Schroeder, W.H., Kemp, R.J., Dias, G.M., Fitzgerald-Hubble, C.R., Wong, E.K., Halfpenny-Mitchell, L., Gustin, M.S., 2001. Sources of variability in mercury flux measurements. J. Geophys. Res. 106, 5421–5435.

Engle, M.A., Gustin, M.S., Zhang, H., 2001. Quantifying natural source mercury emissions from the Ivanhoe Mining District, northcentral Nevada, USA. Atmos. Environ. 35, 3987–3997.

EU, 2017. Regulation 2017/852 of the European Parliament and of the Council of 17 May 2017 on mercury, and repealing regulation (EC) No 1102/2008 (text with EEA relevance.). Orkesterjournalen L 137 (24.25), 21.

FOEN, 2017. Switzerland's Informative Inventory Report 2017. Submission under the UNECE Convention on Long-Range Transboundary Air Pollution. Submission of March 2017 to the United Nations ECE Secretariat. Federal Office for the Environment FOEN. Air Pollution Control and Chemicals Division. Bern.

ForumUmwelt, A.G., 2011. Voruntersuchung von Belasteten Standorten Historische Untersuchung: Objekt 702 Grossgrundkanal, Visp, Schweiz, August 2011.

Frescholtz, T.F., Gustin, M.S., 2004. Soil and foliar mercury emission as a function of soil concentration. Water Air Soil Pollut. 155, 223–237.

Frossard, A., Donhauser, J., Mestrot, A., Gygax, S., Bååth, E., Frey, B., 2018. Long- and short-term effects of mercury pollution on the soil microbiome. Soil Biol. Biochem. 120, 191–199.

Gilli, R.S., Karlen, C., Weber, M., Rüegg, J., Barmettler, K., Biester, H., Boivin, P., Kretzschmar, R., 2018. Speciation and mobility of mercury in soils contaminated by legacy emissions from a chemical factory in the Rhône valley in canton of Valais, Switzerland. Soil Systems 2, 44.

Grangeon, S., Guédron, S., Asta, J., Sarret, G., Charlet, L., 2012. Lichen and soil as indicators of an atmospheric mercury contamination in the vicinity of a chlor-alkali plant (Grenoble, France). Ecol. Indicat. 13, 178–183.

Grigg, A.R.C., Kretzschmar, R., Gilli, R.S., Wiederhold, J.G., 2018. Mercury isotope signatures of digests and sequential extracts from industrially contaminated soils and sediments. Sci. Total Environ. 636, 1344–1354.
Guédron, S., Grangeon, S., Jouravel, G., Charlet, L., Sarret, G., 2013. Atmospheric mercury incorporation in soils of an area impacted by a chlor-alkali plant (Grenoble, France): contribution of canopy uptake. Sci. Total Environ. 445, 356–364.
Gustin, M.S., Biester, H., Kim, C.S., 2002. Investigation of the light-enhanced emission of mercury from naturally enriched substrates. Atmos. Environ. 36, 3241–3254.
Horowitz, H.M., Jacob, D.J., Amos, H.M., Streets, D.G., Sunderland, E.M., 2014. Historical Mercury releases from commercial products: global environmental implications. Environ. Sci. Technol. 48, 10242–10250.
Jiang, T., Skyllberg, U., Wei, S., Wang, D., Lu, S., Jiang, Z., Flanagan, D.C., 2015. Modeling of the structure-specific kinetics of abiotic, dark reduction of Hg(II) complexed by O/N and S functional groups in humic acids while accounting for time-dependent structural rearrangement. Geochem. Cosmochim. Acta 154, 151–167.
Jiskra, M., Wiederhold, J.G., Skyllberg, U., Kronberg, R.-M., Hajdas, I., Kretzschmar, R., 2015. Mercury deposition and Re-emission pathways in boreal forest soils investigated with Hg isotope signatures. Environ. Sci. Technol. 49, 7188–7196.
Kim, K.H., Kim, M.Y., 1999. The exchange of gaseous mercury across soil-air interface in a residential area of Seoul, Korea. Atmos. Environ. 33, 3153–3165.
Kocman, D., Horvat, M., Pirrone, N., Cinnirella, S., 2013. Contribution of contaminated sites to the global mercury budget. Environmental Research, Environ Res 125, 160–170.
Kostka, J.E., Luther, G.W., 1994. Partitioning and speciation of solid phase iron in saltmarsh sediments. Geochem. Cosmochim. Acta 58, 1701–1710.
Larose, C., Prestat, E., Cecillon, S., Berger, S., Malandain, C., Lyon, D., Ferrari, C., Schneider, D., Dommergue, A., Vogel, T.M., 2013. Interactions between snow chemistry, mercury inputs and microbial population dynamics in an arctic snowpack. PLoS One 8, e79972.
Lin, C.C., Yee, N., Barkay, T., 2011. Microbial transformations in the mercury cycle. In: Liu, G., Cai, Y., O'Driscoll, N. (Eds.), Environmental Chemistry and Toxicology of Mercury.
Lin, C.-J., Zhu, W., Li, X., Feng, X., Sommar, J., Shang, L., 2012. Novel dynamic flux chamber for measuring air–surface exchange of Hg^0 from soils. Environ. Sci. Technol. 46, 8910–8920.
Lin, C.J., Gustin, M.S., Singhasuk, P., Eckley, C., Miller, M., 2010. Empirical models for estimating mercury flux from soils. Environ. Sci. Technol. 44, 8522–8528.
Miller, M.B., Gustin, M.S., 2013. Testing and modeling the influence of reclamation and control methods for reducing nonpoint mercury emissions associated with industrial open pit gold mines. J Air Waste Manage 63, 681–693.
Moore, C., Carpi, A., 2005. Mechanisms of the emission of mercury from soil: role of UV radiation. J. Geophys. Res. 110.
Moore, C.W., Castro, M.S., 2012. Investigation of factors affecting gaseous mercury concentrations in soils. Sci. Total Environ. 419, 136–143.
Navratil, T., Simecek, M., Shanley, J.B., Rohovec, J., Hojdova, M., Houska, J., 2017. The history of mercury pollution near the Spolana chlor-alkali plant (Neratovice, Czech Republic) as recorded by Scots pine tree rings and other bioindicators. Sci. Total Environ. 586, 1182–1192.
Osterwalder, S., Sommar, J., Åkerblom, S., Jocher, G., Fritsche, J., Nilsson, M.B., Bishop, K., Alewell, C., 2018. Comparative study of elemental mercury flux measurement techniques over a Fennoscandian boreal peatland. Atmos. Environ. 172, 16–25.
Outridge, P.M., Mason, R.P., Wang, F., Guerrero, S., Heimbürger-Boavida, L.E., 2018. Updated global and oceanic mercury budgets for the united nations global mercury assessment 2018. Environ. Sci. Technol. 52, 11466–11477.
Poissant, L., Pilote, M., Casimir, A., 1999. Mercury flux measurements in a naturally enriched area: correlation with environmental conditions during the Nevada Study and Tests of the Release of Mercury from Soils (STORMS). J. Geophys. Res. 104, 21845–21857.
Reis, A.T., Rodrigues, S.M., Araújo, C., Coelho, J.P., Pereira, E., Duarte, A.C., 2009. Mercury contamination in the vicinity of a chlor-alkali plant and potential risks to local population. Sci. Total Environ. 407, 2689–2700.
Rinklebe, J., During, A., Overesch, M., Wennrich, R., Stärk, H.-J., Mothes, S., Neue, H.-U., 2009. Optimization of a simple field method to determine mercury volatilization from soils - examples of 13 sites in floodplain ecosystems at the Elbe River (Germany). Ecol. Eng. 35, 319–328.
Seinfeld, J.H., Pandis, S.N., 1998. Meteorology of the local scale. In: Atmospheric Chemistry and Physics: from Air Pollution to Climate Change, second ed.
Shetaya, W.H., Osterwalder, S., Bigalke, M., Mestrot, A., Huang, J.-H., Alewell, C., 2017. An isotopic dilution approach for quantifying mercury lability in soils. Environ. Sci. Technol. Lett. 4, 556–561.
Sprovieri, F., Pirrone, N., Bencardino, M., D'Amore, F., Carbone, F., Cinnirella, S., Mannarino, V., Landis, M., Ebinghaus, R., Weigelt, A., Brunke, E.-G., Labuschagne, C., Martin, L., Munthe, J., Wängberg, I., Artaxo, P., Morais, F., Barbosa, H.D.M.J., Brito, J., Cairns, W., Barbante, C., Diéguez, M.D.C., Garcia, P.E., Dommergue, A., Angot, H., Magand, O., Skov, H., Horvat, M., Kotnik, J., Read, K.A., Neves, L.M., Gawlik, B.M., Sena, F., Mashyanov, N., Obolkin, V., Wip, D., Feng, X.B., Zhang, H., Fu, X., Ramachandran, R., Cossa, D., Knoery, J., Marusczak, N., Nerentorp, M., Norstrom, C., 2016. Atmospheric mercury concentrations observed at ground-based monitoring sites globally distributed in the framework of the GMOS network. Atmos. Chem. Phys. 16, 11915–11935.
Suchara, I., Sucharová, J., 2008. Mercury distribution around the Spolana chlor-alkali plant (central Bohemia, Czech Republic) after a catastrophic flood, as revealed by bioindicators. Environ. Pollut. 151, 352–361.
UN Environment, 2013. Minamata convention on mercury. available at: http://www.mercuryconvention.org. (Accessed 20 March 2019), 71 pp.
UN Environment, 2019. Global Mercury Assessment 2018. UN Environment Programme. Chemicals and Health Branch Geneva, Switzerland.
VBBo, 1998. Verordnung über Belastungen des Bodens. VBBo, Bern, Switzerland, 1998.
Wallschläger, D., Kock, H.H., Schroeder, W.H., Lindberg, S.E., Ebinghaus, R., Wilken, R.-D., 2002. Estimating gaseous mercury emissions from contaminated floodplain soils to the atmosphere with simple field measurement techniques. Water Air Soil Pollut. 135, 39–54.
Wang, S., Feng, X., Qiu, G., Wei, Z., Xiao, T., 2005. Mercury emission to atmosphere from Lanmuchang Hg–Tl mining area, Southwestern Guizhou, China. Atmos. Environ. 39, 7459–7473.
WHO, 2000. WHO air quality guidelines for Europe, chapter 6.9, 2nd edition, WHO Regional Office for Europe, Copenhagen, Denmark.
WHO, 2003. Environmental Mercury and Inorganic Mercury Compounds: Human Health Aspects available at: https://www.who.int/ipcs/publications/cicad/en/cicad50.pdf. (Accessed 20 March 2019).
Wiatrowski, H.A., Ward, P.M., Barkay, T., 2006. Novel reduction of mercury(II) by mercury-sensitive dissimilatory metal reducing bacteria. Environ. Sci. Technol. 40, 6690–6696.
Xiao, Z.F., Stromberg, D., Lindqvist, O., 1995. Influence of humic substances of divalent mercury in aqueous solution. Water Air Soil Pollut. 80, 789–798.
Zhu, W., Li, Z., Li, P., Yu, B., Lin, C.-J., Sommar, J., Feng, X., 2018. Re-emission of legacy mercury from soil adjacent to closed point sources of Hg emission. Environ. Pollut. 242, 718–727.